IET Nanodielectrics

ORIGINAL RESEARCH PAPER

Integrated multifunctional properties of polypropylene composites by employing three-dimensional flower-like MgO with hierarchical surface morphology

Jun-Wei Zha[1,2] | **Qi Cheng**[1] | **Jin-Tao Zhai**[1] | **Xingming Bian**[2] | **George Chen**[3] | **Zhi-Min Dang**[4]

[1]School of Chemistry and Biological Engineering, University of Science and Technology Beijing, Beijing, China

[2]State Key Laboratory of Alternate Electrical Power System with Renewable Energy Sources, North China Electric Power University, Beijing, China

[3]School of Electronics and Computer Science, University of Southampton, Southampton, UK

[4]Department of Electrical Engineering, State Key Laboratory of Power System, Tsinghua University, Beijing, China

Correspondence

Jun-Wei Zha, School of Chemistry and Biological Engineering, University of Science and Technology, Beijing No. 30 Xueyuan Road, Haidian District, Beijing 100083, China.
Zhi-Min Dang, Department of Electrical Engineering, Tsinghua University, Beijing 100084, China.
Email: dangzm@tsinghua.edu.cn

Abstract

Polymer nanocomposites have attracted increased attention for use in the field of high-voltage direct current (HVDC) cable insulation. To study the use of polymer nanocomposites for this purpose, 3D flower-like MgO (flower-MgO) particles with hierarchical surface morphology are first synthesised. Polypropylene (PP) was simultaneously mixed with styrene-(ethylene-co-butylene)-styrene triblock copolymer (SEBS) and flower-MgO to obtain PP/SEBS/flower-MgO composites. The microstructural, thermal, electrical, and mechanical properties of the obtained nanocomposites were then studied in detail. The results showed that flower-MgO particles loaded at low concentration were well dispersed in the PP/SEBS matrix. The incorporation of flower-MgO particles has been found to significantly suppress the injection of homocharges and strengthen the ability to release the charge, thus containing accumulation of the space charge. The DC breakdown strength of PP/SEBS/flower-MgO composites was increased to 323 MV/m. Meanwhile, the tensile strength and elongation at break of the obtained composites was improved by loading 0.5 phr flower-MgO because of the synergistic toughening effects of SEBS and MgO. The investigation demonstrates the immense potential to replace nonrecyclable cross-linked polyethylene as an HVDC cable insulating material.

1 | INTRODUCTION

With rapid economic development and increasing demand for electricity, the requirements of ultra-high-voltage, long-distance, and large-capacity transmission lines continue to escalate. Compared with AC transmission systems, DC transmission systems have the advantages of large transmission capacity and long transmission distance. Moreover, power regulation of high-voltage direct current (HVDC) transmission systems is fast and flexible, the risks for a wide range of chain failures are low, and system operation is more reliable. As an essential part of the HVDC transmission system, HVDC cables are widely used in wind power grid connection, island power supply, and cross-sea long distance transmission [1–5]. The critical issues of HVDC cable insulation materials have been further studied to promote the application of HVDC cables in power transmission within large-capacity, long-distance, and complex environments.

With their excellent electrical insulating and mechanical properties, cross-linked polyethylene (XLPE) and its nanocomposites are considered the most popular dielectric materials for commercial HVDC cable insulation [6–11]. However, these materials do not degrade easily because of their thermosetting natures, thus causing an enormous adverse impact

on the environment. In contrast, polypropylene (PP) not only has excellent electrical and heat resistance properties but can also be recycled, making it possible to use it as a replacement for XLPE in cable insulation [12–14]. Isotactic PP is the most extensively studied PP as a thermoplastic in HVDC cable development [15]. Many pieces of research have focussed on PP to significantly improve electrical properties [16, 17]. However, poor mechanical properties limit PP's application. Many investigations have focussed on modifying PP's mechanical properties, the most effective way being to blend it with other thermoplastic elastomers, such as styrene-(ethylene-co-butylene)-styrene triblock copolymer (SEBS) and polyolefin elastomer [18, 19]. Also, the accumulation of space charge is very likely to occur in the polymer insulating materials of HVDC cable, especially in the presence of high electric fields [20–22]. However, the generation, existence, transfer and even disappearance of space charge changes the distribution of the electric field materials and ultimately affects insulating properties [23, 24]. Thus, the space charge is a critical issue limiting the application of HVDC cables. At present, introducing some organic or inorganic nanoparticles into the polymer material has been found to have outstanding effects on the suppression of space charge and is currently a major research hot spot. Different types of metal oxides with several dimensions and various sizes of fillers, such as MgO, ZnO, AlO_3, SiO_2, and TiO_2 [25–31] have been investigated. However, only a few studies have investigated whether the filling of nanocomposites with oxides of hierarchical structure can suppress the space charge and its mechanism. Pourrahimi et al. [32] introduced highly efficient interfaces in nanocomposites based on polyethylene and ZnO nano/hierarchical particles to achieve ultra-low conductivity. Wu et al. [33] synthesised two types of 3D ZnO (flower-like and walnut-like) composites, and the dielectric constant of ZnO filled poly(vinylidene fluoride) composites was found to increase severalfold, which was attributed to the formation of a percolation network of ZnO.

This work studies 3D flower-like MgO with hierarchical surface morphology prepared via a template-free solvothermal method. The selected SEBS as a modifier was added to PP, which plays the role in synergistic toughening and improving the problems of low-temperature impact toughness. The PP/SEBS/flower-MgO composites were prepared by melt blending, and the effects of flower-MgO on the electrical properties of composites were investigated. Moreover, the formation mechanism of the hierarchical structure is systematically discussed.

2 | EXPERIMENTAL

2.1 | Materials

PP (K1008) with a tensile yield strength of 31 MPa and a melt flow index of 10 g/10 min was purchased from Beijing Yanshan Petrochemical Company. SEBS 6150 was supplied from TSRC (Nantong, China) Industries Ltd.

2.2 | Preparation of flower-like hierarchical MgO

The light magnesium oxide powder was added to an aqueous magnesium chloride solution with stirring in a water bath at 50°C for 1 h. Then, the precipitation of magnesium chloride was obtained by ageing at room temperature for 48 h. The resultant precipitate was suction-filtered and washed three times with deionised water and isopropanol, respectively. The washed and filtered precipitate was dried in an oven (80°C, 3 h) to obtain a white magnesium chloride sample. Similarly, the precursor magnesium chloride was added to sodium hydroxide with stirring at 60°C in a water bath for 1 h. The reaction system was aged at room temperature for 14 h to obtain a magnesium hydroxide precipitate that was then washed with deionised water and absolute ethanol to remove Na^+, Cl^-, and other impurities. The washed and filtered precipitate was dried in an oven (80°C, 3h) to obtain white magnesium hydroxide. By employing the precursor thermal decomposition method, the magnesium hydroxide was calcined in a muffle furnace to obtain magnesium oxide. The calcination for the preparation of magnesium oxide was achieved by employing a calcination temperature of 400°C at a heating rate of 3°C/min for 1 h.

2.3 | Preparation of polypropylene/styrene-(ethylene-co-butylene)-styrene triblock copolymer/flower-MgO composites

The PP/SEBS/flower-MgO composites were prepared by melt blending. The flower-MgO, PP, and SEBS pellets were mixed using an RM-200C torque rheometer (HAPRO, Harbin, China) at 190°C for 15 min at a rotor speed of 60 rpm. The weight fractions of the flower-MgO nanoparticles were 0, 0.5, 1.0, and 3.0 phr (where 1.0 phr indicates 1 g of flower-MgO particles in 100 g of PP/SEBS blends, and the content of SEBS in 100 g of PP/SEBS blends is 35 g). Finally, the samples were obtained by hot pressing at 190°C for 20 min under a pressure of about 15 MPa, and the samples were then cooled to room temperature for 5 min. The obtained samples have different thicknesses to test different performances.

2.4 | Characterisation

The morphology and microstructure of flower-like hierarchical MgO fillers and their nanocomposites were observed by scanning electron microscopy (SEM, SU8010 Hitachi, Japan). X-ray diffraction (XRD) patterns were obtained on an Empyrean X-ray diffractometer (PANalytical, Netherlands) using Cu Kα radiation. Thermal properties of the samples were determined through differential scanning calorimetry (DSC) at a heating rate of 10°C/min after eliminating the thermal history. Space charge distribution of the films was measured using the pulsed electroacoustic method under a DC electric field of 60 MV/m for 90 min at room temperature. The semiconductive material was used as an anode (the upper electrode), and aluminium was used
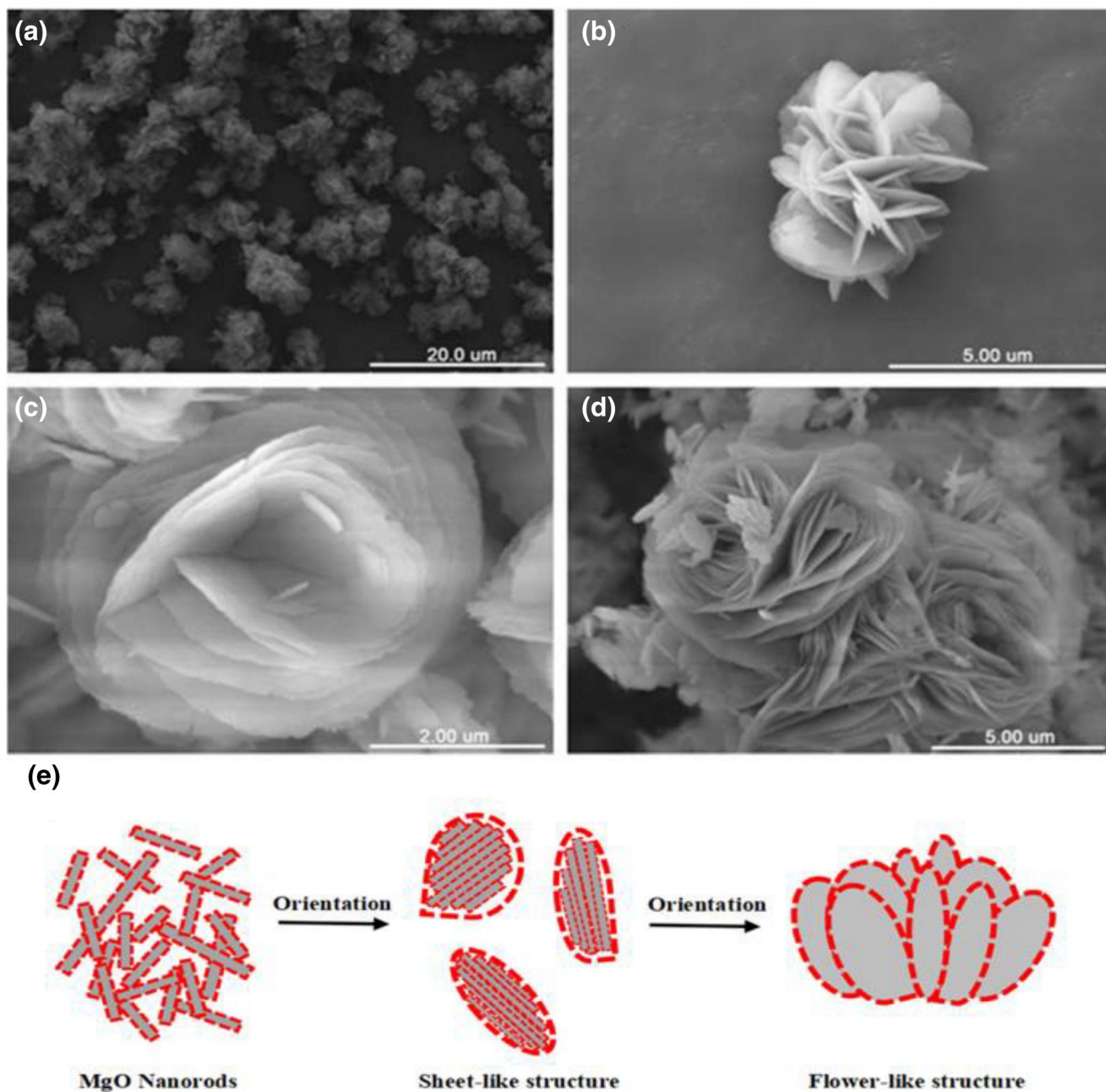
FIGURE 1 (a)–(d) Scanning electron microscopy images of the flower-MgO particles with different scales, and (e) the schematic diagram showing the formation of flower-MgO

as a cathode (the lower electrode). Dielectric properties of the nanocomposites were tested by a precision impedance analyser (Agilent 4294A) within a frequency range of 10^3 to 10^6 Hz. Before measurements, a silver paste was applied on both sides of the PP/SEBS/flower-MgO nanocomposite films to ensure good electrical contact. DC breakdown strength was measured using a sphere-to-sphere copper electrode instrument. The films, with an average thickness of 150 μm, were immersed in silicone oil to isolate them from air and control the temperature, which as placed in the middle of copper electrodes to ensure the occurrence of breakdown at the measuring points when DC voltage was applied. Mechanical properties were measured by a

universal tensile testing machine, and for this, the samples were made into a dumbbell shape.

3 | RESULTS AND DISCUSSION

3.1 | Morphology of flower-MgO particles

Figure 1a–d shows the structure of flower-MgO particles. MgO with flower-like hierarchical structure was synthesised by a liquid phase and precursor decomposition methods, and the size of MgO was about 5 μm. The flower-MgO was composed
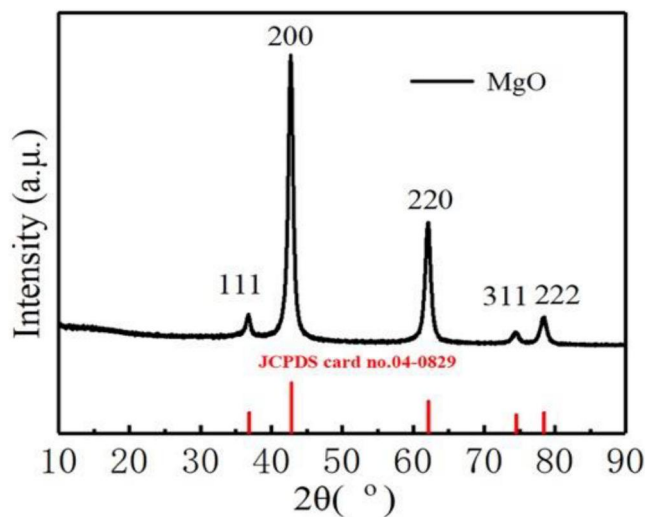
FIGURE 2 X-ray diffraction patterns of the obtained flower-MgO

of basic units with a thickness of 60–80 nm. Due to the initial nucleation stage, the system contains a large number of nanoparticles that have a large specific surface area and collision frequency and thus form a compact structure [34]. MgO nanorods are the smallest fundamental unit of the flower-like structure and first assemble from a free sheet, and then the sheet-like structure constitutes a flower-like structure, as shown in Figure 1e.

Figure 2 shows the XRD patterns of flower-MgO particles. It can be seen that each diffraction peak of the sample is in agreement with the standard PDF card (JCPDS: 04-0829). The characteristic peaks with 2θ values of 36.9, 42.9, 62.3, 74.6, and 78.6 correspond to the (111), (200), (220), (311), and (222) planes of MgO crystal, respectively. These obtained sharp diffraction peaks indicate a high degree of crystallinity. The XRD pattern does not show any impurity peaks, indicating that the process of ageing and washing is adequate.

3.2 | Dispersion and morphology of polypropylene/styrene-(ethylene-co-butylene)-styrene triblock copolymer/flower-MgO composites

Figure 3 shows cross-sectional scanning electron microscopy images of PP/SEBS/flower-MgO composites. It can be seen from Figure 3a that SEBS can be well dispersed in the PP matrix. When the content of flower-MgO in the composites was 0.5 phr and 1.0 phr, there was almost no occurrence of agglomeration, and the dispersion of flower-MgO was relatively uniform. Studies have shown that the particles can introduce traps into the polymer matrix and that particle content has a direct effect on the concentration of traps, which can reduce the electrical properties of the material at higher trap concentrations [35, 36]. It is apparent that when the content of flower-MgO is 3.0 phr, it can be observed that the

basic unit falls off in MgO (Figure 3d), and such a failure of the basic units of nanoparticles will have an impact on their performance.

3.3 | Crystallization characteristics of polypropylene/styrene-(ethylene-co-butylene)-styrene triblock copolymer/flower-MgO composites

Generally, DSC is useful to understand the crystallization process of blends and to obtain a more relevant melting point and crystallinity. The crystallization process is usually composed of two stages, namely, nucleation and growth of grains. The growth of crystal grains depends on the crystallization temperature [37]. X_c is related to melting enthalpy (ΔH_f) and the mass fraction (ϕ) of the polymer matrix in the nanocomposite films, which can be obtained as shown in the following Equation (1) [38]:

$$X_C = \frac{\Delta H_f}{\Delta H_c \times \phi} \times 100\%$$

(1)

where ΔH_c is the melting enthalpy when complete crystallization occurs, which is at about 165 J/g.

Figure 4 shows the crystallization and melting behaviours of the composites. It can be seen that the melting temperature of PP is about 168°C, the melting peak of the composite is nearly 162°C, and the cooling peak is about 115°C, all of which indicate that the added flower-MgO and SEBS have little effect on the melting point of PP and exhibits that the interface between the polymer matrix and the particles is improved. As shown in Table 1, the X_c of the composites is between 30 and 40. The addition of MgO assists the heterogeneous nucleation. However, the crystallinity of the composite becomes smaller after the addition of flower-MgO particles, and the crystallinity becomes more significant as the added amount increases. The interaction between the inorganic particles and polymer molecular chain limits the movement of the molecular chain of the polymer, reducing the molecular chain involved in the crystallization and resulting in a decrease in the crystallinity of the polymer. However, when the content of inorganic particles increases to a certain extent, the nucleation mechanism dominates, and the addition of inorganic whiskers to the polymer plays a role in heterogeneous nucleation and also improves the crystallinity of the composites.

3.4 | Space charge of polypropylene/styrene-(ethylene-co-butylene)-styrene triblock copolymer/flower-MgO composites

Figure 5 shows the space charge distribution in the composites with different contents of flower-MgO under an applied DC voltage of 60 MV/m for 90 min. Some heterocharges near the cathode and the anode can be seen in Figure 5a. The space
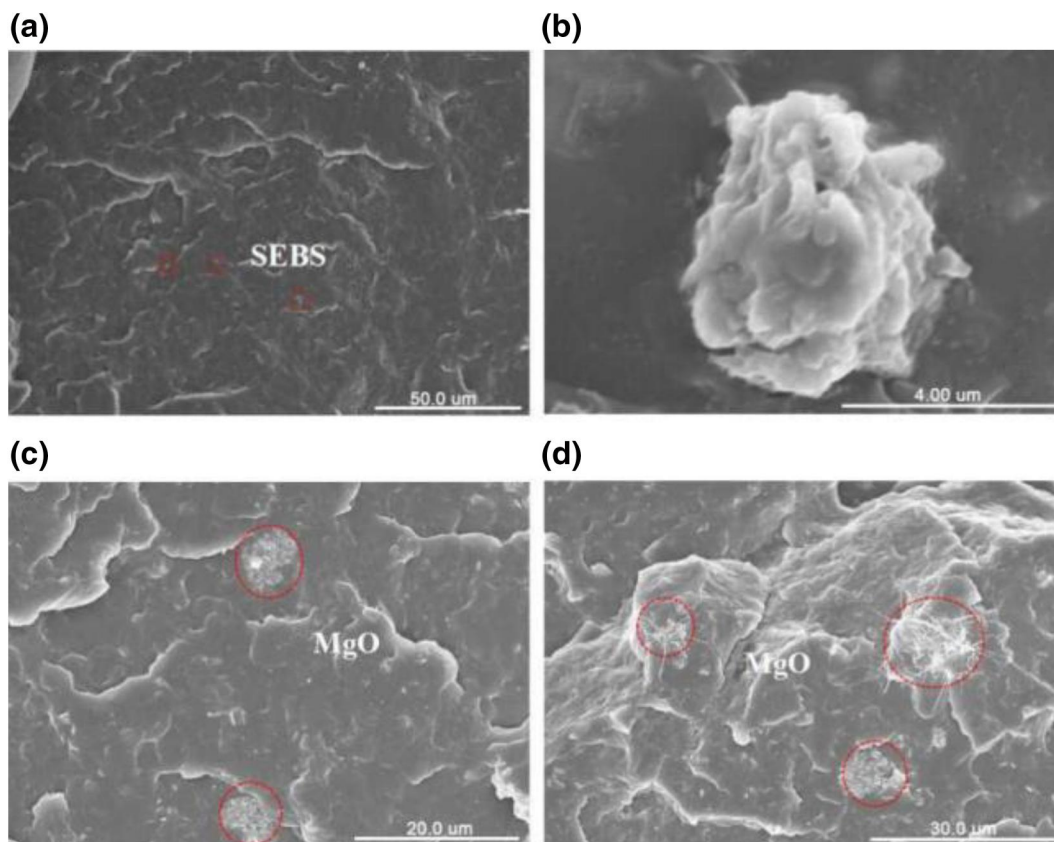
FIGURE 3 Scanning electron microscopy images of polypropylene/styrene-(ethylene-co-butylene)-styrene triblock copolymer/flower-MgO composites with different contents of flower-MgO (a) 0 phr (b) 0.5 phr (c) 1.0 phr and (d) 3.0 phr loading
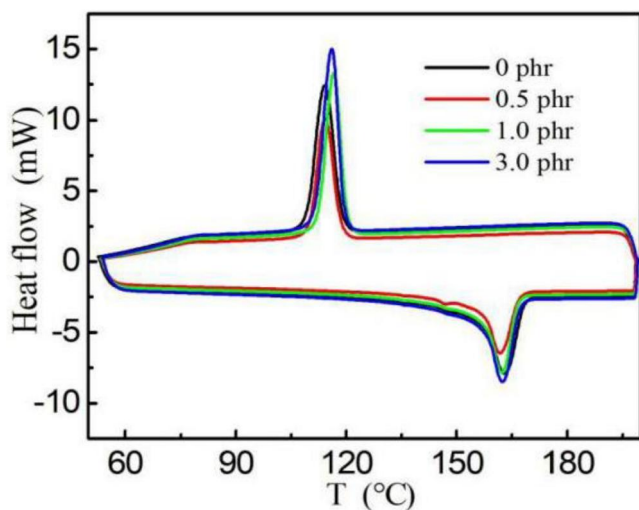

FIGURE 4 Differential scanning calorimetry spectra of polypropylene/styrene-(ethylene-co-butylene)-styrene triblock copolymer/flower-MgO composites

TABLE 1 Differential scanning calorimetry results for the polypropylene/styrene-(ethylene-co-butylene)-styrene triblock copolymer/flower-MgO composite

Flower-MgO content	T_m ($^\circ$C)	Ts ($^\circ$C)	ΔH_f (J/g)	X_c (%)
0 phr	162	115	74.3	45.0
0.5 phr	162	115	58.3	35.5
1.0 phr	162	115	66.9	41.0
3.0 phr	162	116	74.1	46.3

charge continues to accumulate with the increasing volts-on time and remains unchanged at 90 min. This phenomenon may be due to the addition of SEBS, which forms an interface in the interior of the composite, and charge tends to accumulate at the interface, resulting in the accumulation of heterocharges near the electrodes. With an increase in time, the accumulation of charge in the material causes the formation of extra electric field locally. Compared with Figure 5a, almost no space charge accumulation can be seen with the loading of 0.5 phr flower-MgO as shown in Figure 5b, which demonstrates that 0.5 phr flower-MgO can substantially suppress the injection and accumulation of space charge.

When the flower-MgO content is 1.0 phr, it also has a specific effect in suppressing the space charge. It may be because of the addition of filler, which introduces a deep trap, forming a charge adsorption centre, increasing the barrier of electron injection, and reducing the mobility of carriers. However, when flower-MgO is 3.0 phr, the phenomenon of space charge accumulation appears again and becomes more severe than the charge injection of PP/SEBS composites, as
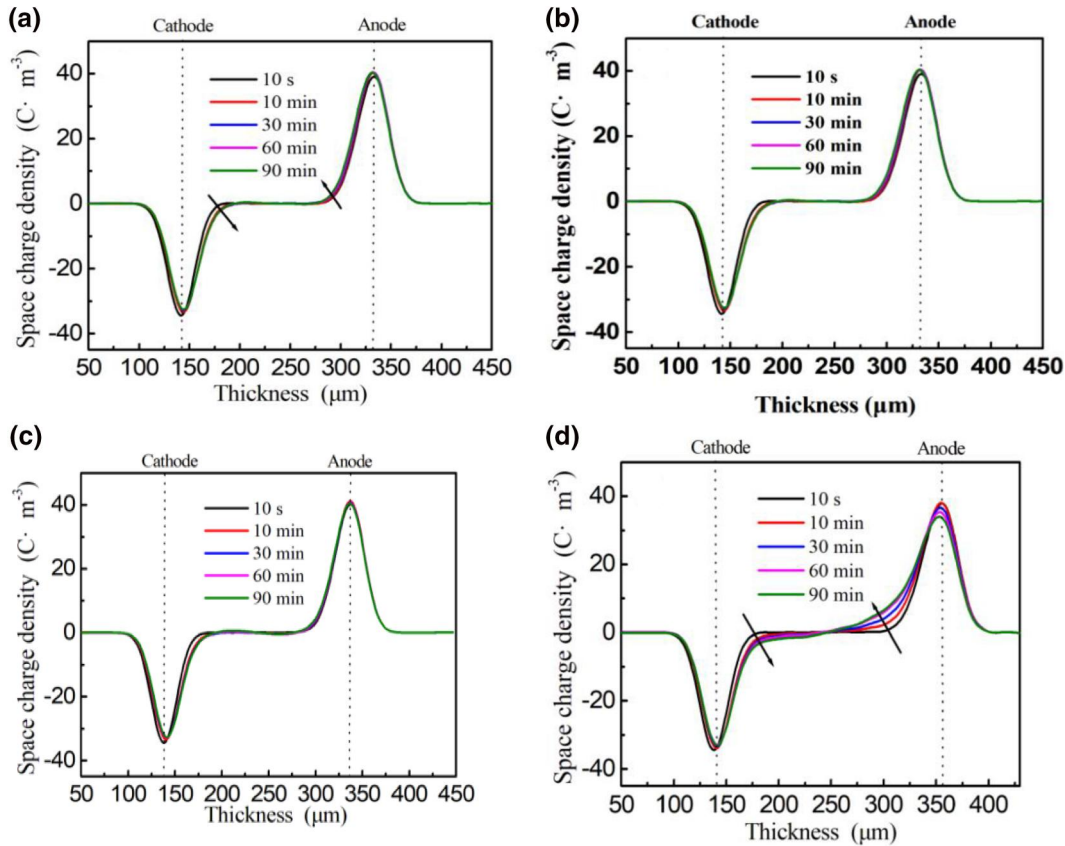
FIGURE 5 Space charge distribution in polypropylene/styrene-(ethylene-co-butylene)-styrene triblock copolymer/flower-MgO composites under an applied electric field of 60 MV/m: (a) 0 phr, (b) 0.5 phr, (c) 1.0 phr, and (d) 3.0 phr flower-MgO loading

shown in Figure 5d. It may be due to the detachment of the basic unit of the particle, introducing a large number of interface defects that are easily formed into a charge centre and accumulate the charge.

Figure 6 shows the corresponding electric field distribution curves after 90 min of polarization under a DC electric field of 60 MV/m. The accumulation of space charges causes a change in the distribution of the nearby electric field, thus resulting in severe distortion in the electric field. The distortion factor is calculated as shown in the following Equation (2):

$$\Delta E = |\frac{E_{max} - E_{av}}{E_{av}}| \times 100\% \qquad (2)$$

where E_{max} is the highest electric field under an electric field of 60 MV/m for 90 min, and an ideal average electric field of E_{av} is 60 MV/m. It can be seen from Figure 6 that the distortion electric fields are 5.9, 4.2, 5.1, and 11.9 MV/m, which are consistent with the changes in the space charge. As shown in Figure 6a, the accumulation of heteropolar space charge in the interface increases the electric field near the interface, which causes the electric field to be distorted with a distortion factor of 9.8%. This is very destructive for the insulation of HVDC cable insulation. In Figure 6b, electric field distortion is significantly reduced due to the formation of deep traps that are caused by the introduction

of particles. These deep traps can adequately capture the carriers and reduce the migration of carriers inside the material, thereby suppressing the space charge and reducing electric field distortion. Similarly, the addition of 1.0 phr of flower-MgO also reduced the electric field distortion. However, as shown in Figure 6d, in the case of a large content of flower-MgO, the electric field distortion is significantly increased, and the distortion factor is 19.8%. This is mainly because of the formation of increased traps by the interface with the substrate, and because the conductive path is easily formed with the high content of fillers. Therefore, the accumulation of space charge increases significantly, and the corresponding electric field distortion is also severe. At the same time, it is also related to the occurrence of interface defects due to the falling off the basic units of the particles.

Figure 7 shows the decay curve of charge when depolarised after pressing the PP/SEBS/flower-MgO composites for 90 min. It can be seen from Figures 7b,c that the charge inside the material quickly dissipates, and the amount of charge accumulation inside the composite with 0.5 phr flower-MgO becomes the least. This shows that during the process of depolarisation, the charge easily overcomes the barrier, jumps from the trap region, and migrates to the outside. However, when the flower-MgO content reaches 3.0 phr, the charge in the body does not substantially dissipate.
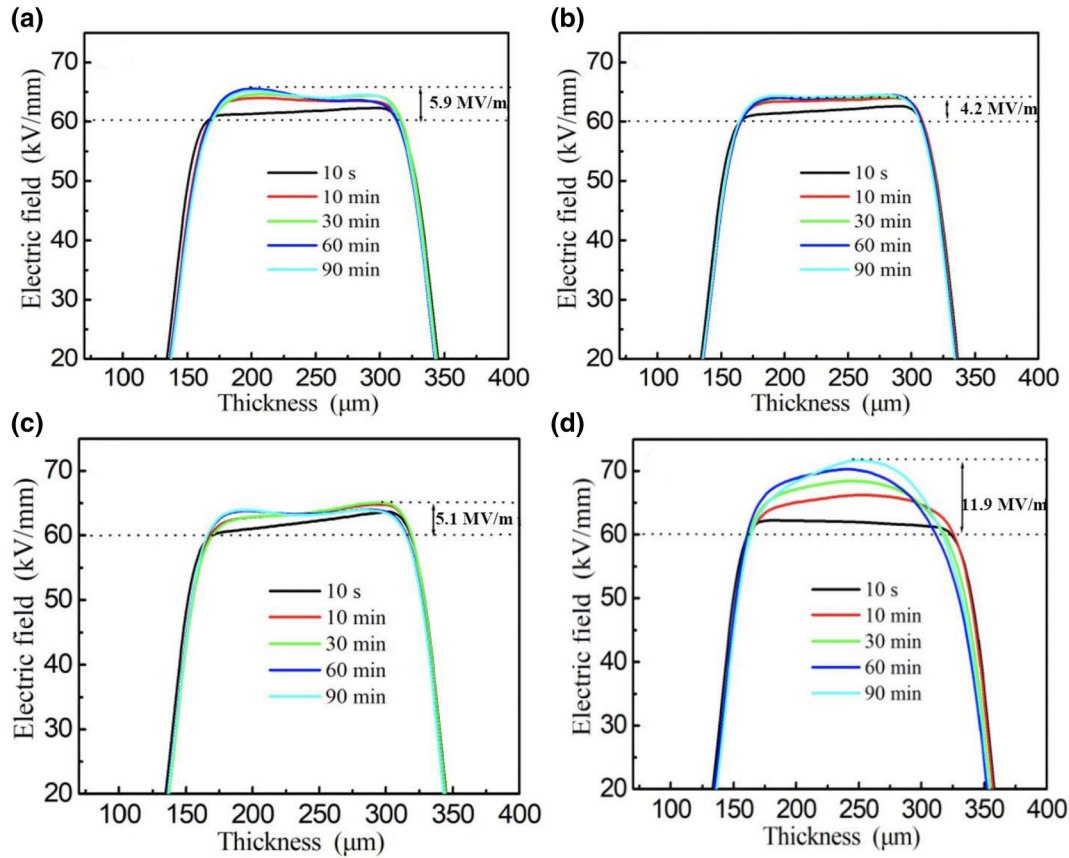
FIGURE 6 The electrical field distribution of polypropylene/styrene-(ethylene-co-butylene)-styrene triblock copolymer/flower-MgO composites under an applied electric field of 60 MV/m for 90 min: (a) 0 phr, (b) 0.5 phr, (c) 1.0 phr, and (d) 3.0 phr flower-MgO loading

Due to the defect in the filler, there is a rod-like tip that readily concentrates the charge. The interface defects of the polymer matrix make the composites less capable of releasing the electric charge and the largest amount of the charge accumulation.

3.5 | Breakdown strength of polypropylene/ styrene-(ethylene-co-butylene)-styrene triblock copolymer/flower-MgO composites

The breakdown strength of PP/SEBS/flower-MgO composites is analysed within the framework of Weibull statistics, and the thicknesses of all the samples are about 150 μm. The distributions for the electrical breakdown include Weibull, Gumbel, and lognormal. The most common for solid insulation is Weibull, which reflects the probability of the material at a particular field strength (E) or the probability of failure or breakdown at a certain time (t). The expression for the cumulative density function for the two-parameter Weibull distribution is shown as follows (Equation (3)):

$$P = 1 - \exp\left[-\left(\frac{E}{\alpha}\right)^{\beta}\right] \tag{3}$$

where P is the cumulative probability of the breakdown, E is the breakdown strength for testing, β is the shape factor reflecting the dispersion of data, and α is the characteristic breakdown strength when the cumulative probability of dielectric breakdown is 63.2%. The logarithmic transformation of the formula has been considered twice, and the following Equation (4) is obtained:

$$\log[-\ln(1 - P)] = \beta \log(E) - \beta \log(\alpha) \tag{4}$$

where $\log[-\ln(1-P)]$ and $\log(E)$ reveal a linear relationship in the Cartesian coordinate system. According to IEEE Standard 930-2004, when the number of samples is less than 25, this can be further simplified as follows (Equation (5)) [39]:

$$P_i = \frac{i - 0.44}{n + 0.25} \times 100\% \tag{5}$$

where n is testing times for each sample, i is the voltage in order from smallest to largest, and a rank from $i = 1$ to $i = n$ has been assigned. It can be seen from Figure 8 that the composite with the loading of 0.5 phr flower-MgO has the highest breakdown strength at 323 MV/m. This is due to the addition of the proper amount of flower-MgO to
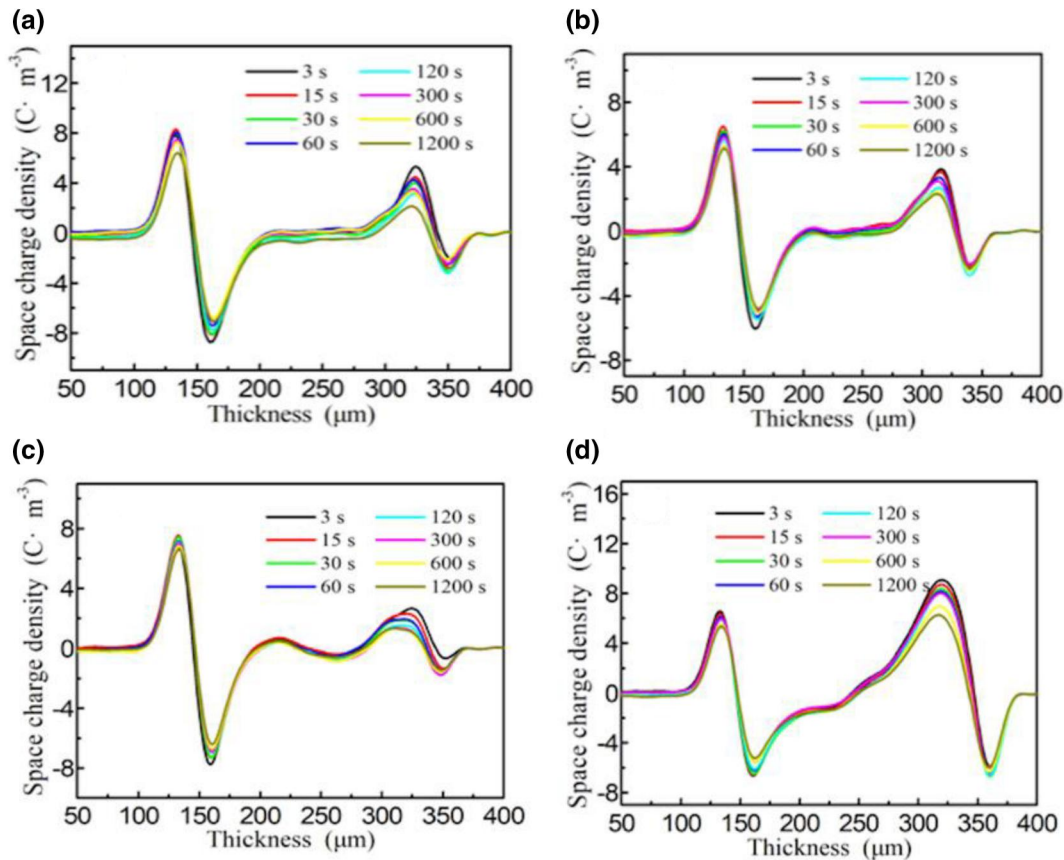
FIGURE 7 The decay curve of charge when depolarised after pressing polypropylene/styrene-(ethylene-co-butylene)-styrene triblock copolymer/flower-MgO composites for 90 min

introduce a deep trap to capture carriers effectively. The molecular chain of the polymer and the surface gap of the filler are well bonded, so the filler becomes a charge adsorption centre, blocks electron migration, increases the jump barrier, and thereby improves breakdown strength. When the content continues to increase, the breakdown strength of the composites decreases. When the flower-MgO content is 3.0 phr, the breakdown strength is lower than that of the PP/SEBS blends. Due to the excessive concentration, the composite generates interface defects, and the breakdown strength is reduced. The laws of action and space charge are consistent, and the accumulation of charge leads to a decrease in the breakdown.

3.6 | Dielectric properties of the polypropylene/styrene-(ethylene-co-butylene)-styrene triblock copolymer/flower-MgO composites

Dielectric properties of the PP/SEBS/flower-MgO composites versus frequency at room temperature are shown in Figure 9. It can be seen from Figure 9a that the PP/SEBS/flower-MgO composite has a stable dielectric permittivity in the frequency range of 103 to 106 Hz, indicating that the
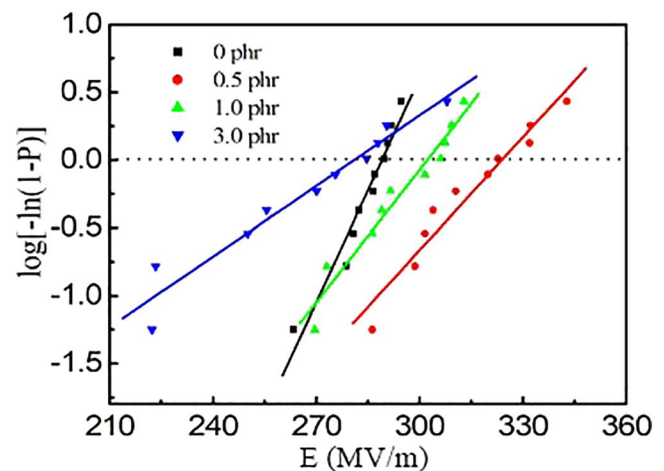

FIGURE 8 Weibull distribution plot for the breakdown strength of the polypropylene/styrene-(ethylene-co-butylene)-styrene triblock copolymer/flower-MgO composites

composites have a wide range of suitable frequencies. Meanwhile, the dielectric permittivity of the composite increases with increasing content of flower-MgO. It can be seen that the dielectric loss increases slightly after the introduction of flower-MgO as shown in Figure 9b, while the values of
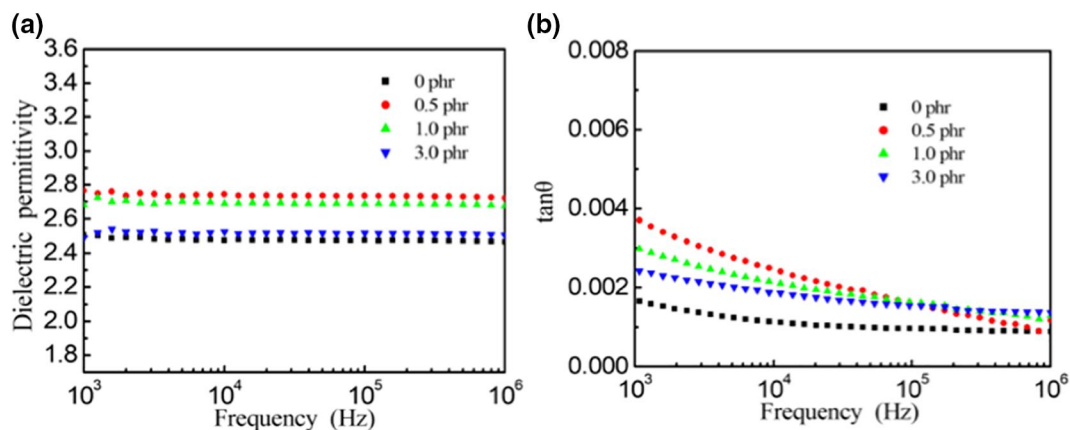
FIGURE 9 Frequency dependence of the (a) dielectric permittivity and (b) dielectric loss tangent of polypropylene/styrene-(ethylene-co-butylene)-styrene triblock copolymer/flower-MgO composites with different contents of flower-MgO
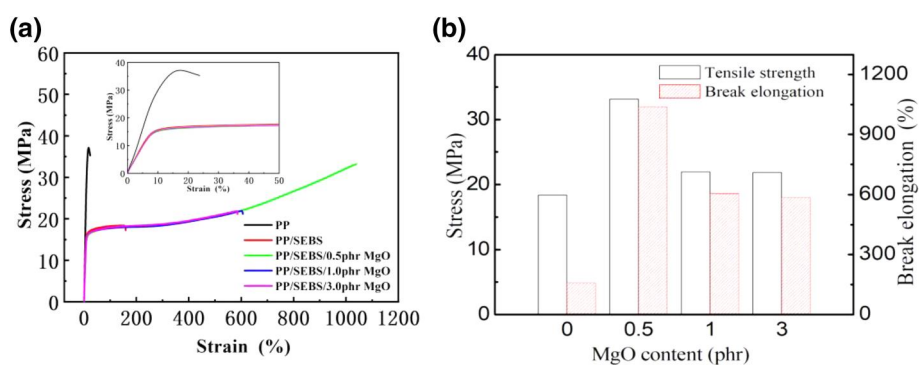

FIGURE 10 Mechanical properties of polypropylene/styrene-(ethylene-co-butylene)-styrene triblock copolymer/flower-MgO composites: (a) typical stress–strain curves; the inner are the stress–strain curves at low strain (b) histogram of tensile strength and elongation at break versus flower-MgO filler content

dielectric losses of the composites are still minimal, generally within 0.004.

3.7 | Mechanical properties of polypropylene/styrene-(ethylene-co-butylene)-styrene triblock copolymer/flower-MgO composites

Figure 10a shows the stress–strain curves of PP, PP/SEBS, and PP/SEBS/flower-MgO composites, and the corresponding tensile strength and elongation at break values are shown in Figure 10b. It can be seen that PP exhibits brittleness and low tensile elongation at break. With the introduction of SEBS, the elongation at break is improved, and it has a specific effect on the toughening of PP. Moreover, as shown in the inner image of Figure 10a, SEBS also decreases the elastic modulus of composites even with the further incorporation of flower-MgO. The tensile strength and elongation at break of PP/SEBS/flower-MgO composites increase with the increasing content of flower-MgO particles. The tensile strength of the composite with 0.5 phr flower-MgO increases to 31.2 MPa compared to the tensile strength of the PP/SEBS blend of 18.4 MPa.

The tensile strength of the composite with 1.0 phr flower-MgO was significantly enhanced to 34.8 MPa. The elongation at break increases from 865% of the PP/SEBS blend to 1040% of the composite with 0.5 phr flower-MgO, then increases to 1098% of the composite with 1.0 phr flower-MgO. From Figure 10b, synergistic toughening of SEBS and flower-MgO particles can be observed. The enhancement of mechanical properties is attributed to the good interfacial compatibility and interfacial adhesion of the filler-polymer in the composite. However, when 3.0 phr flower-MgO particles are introduced, the tensile strength and elongation decrease. The deterioration of mechanical properties is attributed to the defects and stress concentrations caused by the detachment of basic units of the flower-MgO particles.

4 | CONCLUSIONS

In summary, we successfully prepared PP/SEBS/flower-MgO composites using flower-like hierarchical MgO with excellent space charge suppression for HVDC cables. Considering their electrical and mechanical properties, the optimum filler content of PP/SEBS/flower-MgO composites is 0.5 phr flower-MgO. Meanwhil, the composites integrate the complementary

characteristics of various components to inhibit the accumulation of space charge and make the internal charge release ability of the composite material stronger. In addition, DC breakdown strength increases to 323 MV/m. Moreover, tensile strength and elongation at break are much improved. This study provides a way to promote PP as an environmentally friendly material for the research and development of HVDC cables.

ORCID
Jun-Wei Zha https://orcid.org/0000-0003-3301-3505
Xingming Bian https://orcid.org/0000-0003-2706-8251
George Chen https://orcid.org/0000-0002-7271-1368

REFERENCES

1. Jarvid, M., et al.: A new application area for fullerenes: voltage stabilizers for power cable insulation. Adv. Mater. 27(5), 897–902 (2014)
2. Wang, S.J., et al.: Influence of hierarchy structure on electrical properties of gradient-distribution aluminium oxide/polyethylene nanocomposites. Compos. Sci. Technol. 135, 100–105 (2016)
3. Chen, G., et al.: Review of high voltage direct current cables. CSEE J. Power Energy Syst. 1(2), 9–21 (2015)
4. Bresesti, P., et al.: HVDC connection of offshore wind farms to the transmission system. IEEE Trans. Energy Convers. 22(1), 37–43 (2007)
5. Wang, S., et al.: Improved DC performance of crosslinked polyethylene insulation depending on a higher purity. IEEE Trans. Dielectr. Electr. Insul. 24(3), 1809–1817 (2017)
6. Hozumi, N., et al.: Space charge behaviour in XLPE cable insulation under 0.2-1.2 MV/cm dc fields. IEEE Trans. Dielectr. Electr. Insul. 5(1), 82–90 (1998)
7. Wang, Y., et al.: Research progress on space charge measurement and space charge characteristics of nanodielectrics. IET Nanodielectr. 1(3), 114–121 (2018)
8. Zheng, X., Chen, G.: Propagation mechanism of electrical tree in XLPE cable insulation by investigating a double electrical tree structure. IEEE Trans. Dielectr. Electr. Insul. 15(3), 800–807 (2008)
9. Cheng, L., et al.: Polypropylene nanocomposite for power equipment: a review. IET Nanodielectr. 1(2), 92–103 (2018)
10. Densley, R.J.: An investigation into the growth of electrical trees in XLPE cable insulation. IEEE Trans. Electr. Insul. EI-14(3), 148–158 (1979)
11. Ohki, Y.: Development of XLPE-insulated cable for high-voltage dc submarine transmission line (1)'. IEEE Electr. Insul. Maga. 29(4), 65–67 (2012)
12. Zha, J.W., et al.: Morphology and crystalline-phase-dependent electrical insulating properties in tailored polypropylene for HVDC cables. Appl. Phys. Lett. 109, 222902 (2016)
13. Lotz, B., Wittmann, J.C., Lovinger, A.J.: Structure and morphology of poly(propylenes): a molecular analysis. Polymer. 37(22), 4979–4992 (1996)
14. Zha, J.W., et al.: Improvement of space charge suppression of polypropylene for potential application in HVDC cables. IEEE Trans. Dielectr. Electr. Insul. 23(4), 2337–2343 (2016)
15. Diao, J., et al.: Thermoplastic isotactic polypropylene/ethylene-octene polyolefin copolymer nanocomposite for recyclable HVDC cable insulation. IEEE Trans. Dielectr. Electr. Insul. 24(3), 1416–1429 (2017)
16. Yang, J.M., et al.: Space charge characteristics of polypropylene modified by rare earth nucleating agent for β crystallization. Materials. 12(1), 42 (2019)
17. Zhou, Y., et al.: Evaluation of polypropylene/polyolefin elastomer blends for potential recyclable HVDC cable insulation applications. IEEE Trans. Dielectr. Electr. Insul. 22(2), 673–681 (2015)
18. Du, B.X., Xu, H., Li, J.: Effects of mechanical stretching on space charge behaviours of PP/POE blend for HVDC cables. IEEE Trans. Dielectr. Electr. Insul. 24(3), 1438–1445 (2017)
19. Zha, J.W., et al.: Electrical properties of polypropylene/styrene-ethylenebutylene-styrene block copolymer/MgO nanocomposites. IEEE Trans. Dielectr. Electr. Insul. 24(3), 1457–1464 (2017)
20. Montanari, G.C., Morshuis, P.H.F.: Space charge phenomenology in polymeric insulating materials. IEEE Trans. Dielectr. Electr. Insul. 12(4), 754–767 (2005)
21. Ghorbani, H., et al.: Electrical characterisation of extruded DC cable insulation-the challenge of scaling. IEEE Trans. Dielectr. Electr. Insul. 24(3), 1465–1475 (2017)
22. Wu, K., Cheng, C.H.: Interface charges between insulating materials. IEEE Trans. Dielectr. Electr. Insul. 24(4), 2633–2642 (2017)
23. Mizutani, T., Semi, H., Kaneko, K.: Space charge behaviour in low-density polyethylene'. IEEE Trans. Dielectr. Electr. Insul. 7(4), 503–508 (2000)
24. Teyssedre, G., et al.: Interface tailoring for charge injection control in polyethylene. IEEE Trans. Dielectr. Electr. Insul. 24(3), 1319–1330 (2017)
25. Dang, B., et al.: Suppression of elevated temperature space charge accumulation in polypropylene/elastomer blends by deep traps induced by surface-modified ZnO nanoparticles. Compos. Sci. Technol. 153(17), 103–110 (2017)
26. Zha, J.W., et al.: Enhanced dielectric properties and energy storage of the sandwich-structured poly(vinylidene fluoride-co-hexafluoropropylene) composite films with functional BaTiO3@Al2O3 nanofibres. IET Nanodielectr. 2(3), 103–108 (2019)
27. Guo, N., et al.: Nanoparticle, size, shape, and interfacial effects on leakage current density, permittivity, and breakdown strength of metal oxide-polyolefin nanocomposites: experiment and theory. Chem. Mater. 22(4), 1567–1578 (2010)
28. Pourrahimi, A.M., et al.: Polyethylene nanocomposites for the next generation of ultralow-transmission-loss HVDC cables: insulation containing moisture-resistant MgO nanoparticles. ACS Appl. Mater. Interfaces. 8(23), 14824–14835 (2016)
29. Krentz, T., et al.: Morphologically dependent alternating-current and direct-current breakdown strength in silica-polypropylene nanocomposites. J. Appl. Polym. Sci. 134(1), 44347 (2017)
30. Zhang, D.L., et al.: High thermal conductivity and excellent electrical insulation performance in double-percolated three-phase polymer nanocomposites. Compo. Sci. Technol. 144(16), 36–42 (2017)
31. Hidayah, I.N., et al.: Evaluation of PP/EPDM nanocomposites filled with SiO2, TiO2 and ZnO nanofillers as thermoplastic elastomeric insulators'. Plast. Rubber Compos. 44(7), 259–265 (2015)
32. Pourrahimi, A.M., et al.: Highly efficient interfaces in nanocomposites based on polyethylene and ZnO nano/hierarchical particles: a novel approach towards ultralow electrical conductivity insulations. Adv. Mater. 28(39), 8651–8657 (2016)
33. Wu, W., et al.: Novel three-Dimensional zinc oxide superstructures for high dielectric constant polymer composites capable of withstanding high electric field. J. Phys. Chem. C. 116(47), 24887–24895 (2012)
34. Zeng, J., Xia, Y.N.: Hybrid nanomaterials: not just a pretty flower. Nat. Nanotech. 7(7), 415–416 (2012)
35. Zha, J.W., et al.: Mechanism analysis of improved corona-resistant characteristic in polyimide/TiO$_2$ nanohybrid films. Appl. Phys. Lett. 93, 192911 (2008)

36. Mizutani, T.: Space charge measurement techniques and space charge in polyethylene. IEEE Trans. Dielectr. Electr. Insul. 1(5), 923–933 (1994)

37. Du, W.C., et al.: Space charge distribution and crystalline structure in polyethylene blended with EVOH. Europ. Polym. J. 40(8), 1987–1995 (2004)

38. Lu, X., et al.: Characterisations of P(VDF-HFP)-BaTiO3 nanocomposite films fabricated by a spin-coating process. Ceram. Int. 45(14), 17758–17766 (2019)

39. Wang, S.J., et al.: Distinctive electrical properties in sandwich-structured Al_2O_3/low density polyethylene nanocomposites. Appl. Phys. Lett. 108, 092902 (2016)